Spin relaxation mechanism in a highly doped organic polymer film

Motoi Kimata,* Daisuke Nozaki, and Yasuhiro Niimi
Institute for Solid State Physics, University of Tokyo, Kashiwano-ha 5-1-5, Kashiwa, Chiba 277-8581, Japan

Hiroyuki Tajima
Graduate School of Material Science, University of Hyogo, Kouto 3-2-1, Kamigori, Ako, Hyogo 678-1205, Japan

YoshiChika Otani
Institute for Solid State Physics, University of Tokyo, Kashiwano-ha 5-1-5, Kashiwa, Chiba 277-8581, Japan
and Center for Emergent Matter Science (CEMS) RIKEN, 2-1 Hirosawa, Wako, Saitama 351-0198, Japan
(Received 23 October 2014; revised manuscript received 15 May 2015; published 17 June 2015)

We report systematic studies on the spin current transport and relaxation mechanism in thin films of the highly doped organic polymer poly(3,4-ethylenedioxythiophene):poly(styrenesulfonate) (PEDOT:PSS), in which hopping charge transport is dominant. In this study, we determined the spin diffusion length, spin lifetime, and spin diffusion constant using different experimental techniques. The experimentally obtained spin lifetime is much shorter than that of nondoped organic semiconductors. This clearly shows considerable enhancement of spin relaxation in highly doped PEDOT molecules, which form the trapping centers of hopping transport. Also, we obtained a longer spin diffusion length than the average hopping length, indicating that spins are almost conserved during the hopping process. These facts suggest that spin relaxation of this material mainly occurs in the nanograins of the PEDOT molecules.

DOI: 10.1103/PhysRevB.91.224422 PACS number(s): 75.40.Gb, 76.30.−v, 85.65.+h

I. INTRODUCTION

Organic semiconductors (OSCs) have attracted much attention because of their potential applications for field-effect transistors, solar cells, and displays. These applications are stimulated by the unique properties of OSCs: low cost, low weight, and flexibility. Also, OSCs are attractive candidates for spintronic device applications. Spintronics use electron spins as information carriers, and therefore their lifetime and transport length, i.e., spin diffusion length (SDL), are important parameters to design spintronic devices [1]. OSCs generally consist of relatively light elements, such as hydrogen, carbon, and sulfur, in which the spin-orbit (SO) interaction is expected to be weak. Since the SO interaction is the main origin of spin relaxation, OSCs are promising materials for long-distance spin transport [2]. So far, many experiments have been performed to measure the SDLs of OSCs using the magnetoresistance effect between two ferromagnetic electrodes, where spin polarized charge currents pass through the organic layer [3–8]. On the other hand, the pure spin current, with no net charge current, is an essential ingredient of next generation spintronics [9,10]. However, the study of pure spin transport in OSCs is limited and their properties are not yet fully understood because of the lack of complementary information about the spin diffusion constant (D_S) and the spin lifetime (τ_S). For example, recently performed dynamical spin transport experiments suggest quite a long τ_S in OSCs, but their reliability has not been confirmed experimentally [11,12]. To solve this problem, a comprehensive study of OSCs is necessary to determine spin transport parameters.

In the present work, we performed comprehensive studies on spin transport using spin pumping, electron paramagnetic resonance (EPR), and charge transport experiments in a highly doped organic polymer film. From these experiments, we determined the SDL, τ_S, and D_S independently, and deduced the spin transport mechanism in disordered organic polymers.

The organic material used in this study was the conducting polymer poly(3,4-ethylenedioxythiophene): poly(styrenesulfonate) (PEDOT:PSS, Clevios PH1000, Heraeus Precious Metals, Germany). In this material, the conjugated PEDOT polymer is doped with PSS. The morphology and synchrotron x-ray diffraction studies reveal that the PEDOT:PSS film is formed by pancakelike core-shell structures consisting of PEDOT-rich cores surrounded by PSS insulating shells [13,14]. This core-shell structure is 20–30 nm long in the in-plane and 5–6 nm long in the out-of-plane directions.

II. EXPERIMENTAL DETAILS

The device structure for the dynamical spin pumping experiment was a trilayer of $Ni_{81}Fe_{19}$ (permalloy: Py)/PEDOT:PSS/Pt fabricated on a thermally oxidized Si substrate (the thickness of the SiO_2 was 100 nm). After the deposition of a 15 or 8 nm thick Pt layer, a water based PEDOT:PSS layer was spin coated with a variable rotational speed from 1000 to 6000 rpm to change the thickness of the PEDOT:PSS layer. The surface roughness of the PEDOT:PSS film was approximately 3–4 nm determined using atomic force microscopy. The PEDOT:PSS film was annealed at 50 °C in a pressure below 4×10^{-4} Pa for about 10 h, and then the Py layer was deposited in a vacuum on PEDOT:PSS at a rate of ∼0.01 nm/s. The base pressure was approximately 5×10^{-6} Pa. The spin pumping and EPR experiments were performed using a conventional *X*-band EPR spectrometer with a TE_{102} rectangular cavity. The operation frequency was approximately 9.45 GHz and the sample was set at the center of the cavity. Charge transport

*kimata@issp.u-tokyo.ac.jp

measurements were performed using the same trilayer structure with a junction area of 40×100 $(\mu m)^2$.

III. RESULTS AND DISCUSSIONS

Figure 1(a) shows a schematic illustration of the device structure used for our spin pumping experiment. The spin pumping driven by ferromagnetic resonance (FMR) generates pure spin current dissipates into the PEDOT:PSS layer via the exchange interaction at the Py/PEDOT:PSS interface [15–18]. The transmitted spin current across the PEDOT:PSS layer is converted into the orthogonal electric field via the inverse spin Hall (ISH) effect in the Pt layer [18–20]. We can then detect the pure spin current through the PEDOT:PSS layer as a voltage across the Pt layer [Fig. 1(b)]. The upper panel in Fig. 1(c) shows the FMR spectra of a Py strip in the Py(17)/PEDOT:PSS(60)/Pt(8) trilayer device. The numbers in parentheses indicate the film thickness in nanometers. The lower panel of Fig. 1(c) shows the voltage signal $V(H)$ from the Pt layer for $\phi = 0°$. The magnetic field angle ϕ was defined as shown in Fig. 1(a). The solid line is a curve fit to the sum

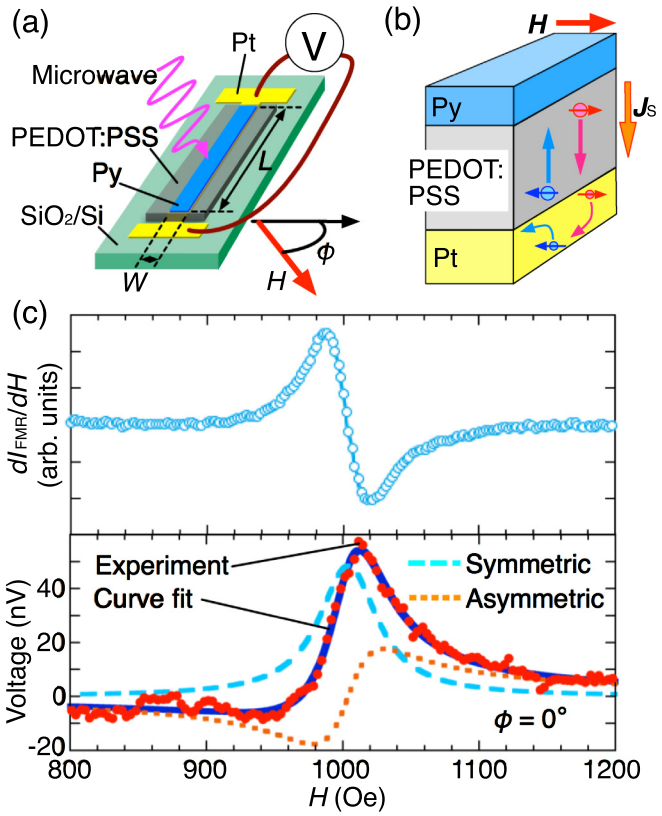

FIG. 1. (Color online) (a) Schematic of the sample structure used for spin transport experiments and (b) the mechanism of spin injection and detection. The injected pure spin current through the PEDOT:PSS layer is absorbed by the Pt layer, and then converted to an electric field via the inverse spin Hall effect. (c) Upper panel: The FMR spectra of the Py strip of Py(17)/PEDOT:PSS(60)/Pt(8) trilayer sample. The numbers in parentheses indicate the film thickness in nanometers. Lower panel: The dc voltage signal at the Pt layer of the trilayer sample for $\phi = 0°$.

of symmetric and asymmetric Lorentz functions,

$$V(H) = \frac{V_S(\Delta H/2)^2}{[(H-H_0)^2+(\Delta H/2)^2]} - \frac{V_A \Delta H(H-H_0)}{[(H-H_0)^2+(\Delta H/2)^2]}, \quad (1)$$

where ΔH is the spectral full width at half maximum and H_0 is the resonance field. V_S and V_A are the symmetric and asymmetric contributions to the voltage signal, respectively [18]. The obtained linewidth and the resonance field are identical to those of FMR spectra, meaning that the voltage signal originates from the FMR of the Py layer. In the present sample structure, two large contributions can be considered to generate the dc voltage signal induced by the FMR. One is the ISH voltage (V_{ISH}) generated along the Pt layer and the other is the voltage induced by the anisotropic magnetoresistance (AMR) effect (V_{AMR}) in the Py layer [21,22]. In spin pumping experiments, the injected spin current has a maximum at H_0. Consequently, V_{ISH} can only contribute to V_S, whereas V_{AMR} can contribute to both V_S and V_A. The origin of V_{AMR} is the interaction between the high frequency electrical current and the magnetization in the Py. In this study, we used a long rectangular Py strip as a spin injector, where the dominant component of the high frequency current is parallel to the long direction. In this case, $V_{AMR} \propto \sin 2\phi$ and thus vanishes when $\phi = 0°$, 90°, and 180° [21,22]. In the case of the ISH effect, the conversion relation between the spin current and electric field is $\boldsymbol{V}_{ISH} \propto \boldsymbol{J}_S \times \boldsymbol{\sigma} \propto \cos\phi$, where $\boldsymbol{J}_S$ is the spin current, and $\boldsymbol{\sigma}$ is the spin polarization vector. Therefore, V_S for $\phi = 0°$ only arises from the ISH effect: $V_S(0°) = V_{ISH}(0°)$ [23,24]. However, the asymmetric voltage contribution still remains for $\phi = 0°$. The origin of this contribution is unclear, but it is attributed to other magnetotransport effects, such as the anomalous Hall effect, planar Hall effect, and spin Hall magnetoresistance, as discussed in recent reports [25–28].

Figure 2(a) shows the magnetic field dependence of the voltage signal for $\phi = 0°$, 90°, and 180°. As shown in the figure, V_S changes its sign depending on the field direction, and vanishes when $\phi = 90°$. Also, the magnitude of V_{ISH} is proportional to the microwave power injected into the cavity [Fig. 2(b)]. Here, we take the average of V_S for $\phi = 0°$ and 180° as V_{ISH}, where $V_{ISH} = [V_S(0°) - V_S(180°)]/2$. These tendencies are consistent with the expected behaviors of V_{ISH} induced by spin pumping [26,29]. The contribution of the PEDOT:PSS layer to V_{ISH} [11] is expected to be quite small in the present sample, and cannot explain the observed V_{ISH} in Fig. 2(a) (see the Supplemental Material [30]). Because the observed V_{ISH} in the Pt layer was generated from the spin current transmitted through the PEDOT:PSS layer, we can estimate the SDL of the PEDOT:PSS from the dependence of V_{ISH} on the PEDOT:PSS thickness (t_{PE}). The plot of normalized V_{ISH} divided by the resistance of the Pt layer (V_{ISH}^N/R_{Pt}) for several values of t_{PE} is shown in Fig. 2(c). To consider the decay of the spin current with t_{PE}, we used the one-dimensional diffusion equation for a trilayer structure with no interface resistance (see the Supplemental Material [30]). Based on our analysis, the spin current at the PEDOT:PSS/Pt

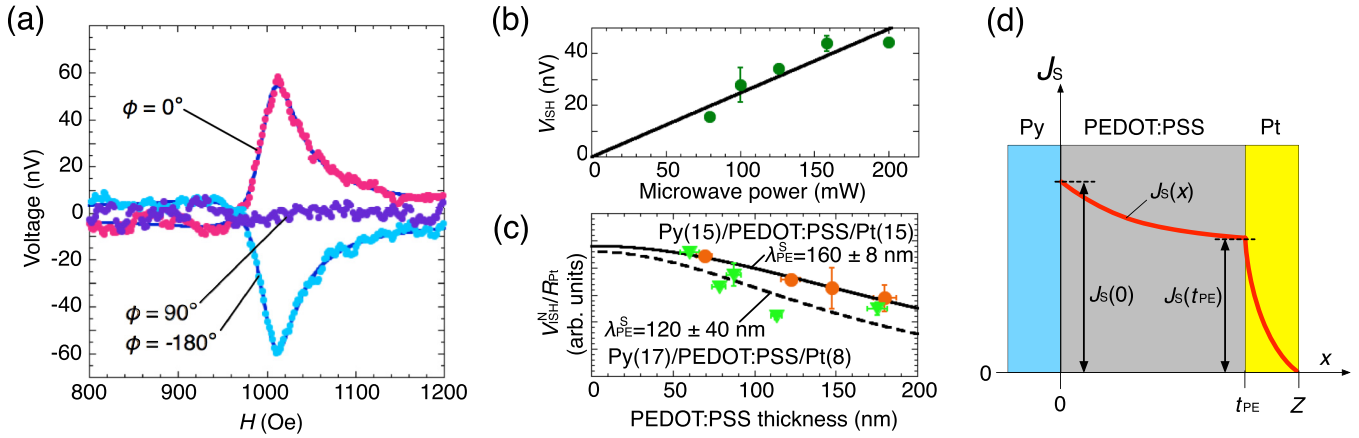

FIG. 2. (Color online) (a) Magnetic field dependence of the voltage signal in Py(17)/PEDOT:PSS(60)/Pt(8) trilayer for $\phi = 0°$, 90°, and 180°. (b) Microwave power dependence of $V_{\rm ISH}$. (c) $V^{\rm N}_{\rm ISH}/R_{\rm Pt}$ as a function of PEDOT:PSS thickness. The solid triangles and circles represent the data for two series of samples. The solid and dashed lines are the fitting results using Eq. (2). (d) Schematic illustration of the decay of the spin current in the present trilayer.

interface [$=J_{\rm S}(t_{\rm PE}) \propto V^{\rm N}_{\rm ISH}/R_{\rm Pt}$] is

$$J_{\rm S}(t_{\rm PE}) \approx J_{\rm S}(0)\exp\left(t_{\rm PE}/\lambda^{\rm S}_{\rm PE}\right)\left[1-\tanh\left(t_{\rm PE}/\lambda^{\rm S}_{\rm PE}\right)\right] \quad (2)$$

for $\rho_{\rm Pt} \ll \rho^{\perp}_{\rm PE}$. Here, $J_{\rm S}(0)$, $\lambda^{\rm S}_{\rm PE}$, $\rho_{\rm Pt}$, and $\rho^{\perp}_{\rm PE}$ are the spin current at $x = 0$ [see Fig. 2(d)], SDL of PEDOT:PSS, and the resistivities of Pt and PEDOT:PSS in the out-of-plane direction, respectively. In the present case, the condition $\rho_{\rm Pt} \ll \rho^{\perp}_{\rm PE}$ is reasonable because their values are $\rho_{\rm Pt} \approx 22\ \mu\Omega\,$cm and $\rho^{\perp}_{\rm PE} \approx 1.0\ {\rm k}\Omega\,$cm, respectively. The decay of the spin current is schematically illustrated by the solid line in Fig. 2(d). The SDL of PEDOT:PSS can be determined by fitting the data in Fig. 2(c) to Eq. (2). The SDLs for the two sets of samples were therefore 160 ± 8 and 120 ± 40 nm. The difference in the SDLs for the two distinct sample sets is because of the difference in resistivity of the PEDOT:PSS films. The average resistivities for the two sample sets are 0.93 ± 0.2 and $1.1 \pm 0.2\ {\rm k}\Omega\,$cm, respectively. The SDL of 140 ± 20 nm on average for PEDOT:PSS obtained from our experiments is longer than the SDL of 21–30 nm reported in the previous study [11], where $\tau_{\rm S}$ was estimated to be 5–10 μs [11]. Therefore, $\tau_{\rm S}$ of our PEDOT:PSS film seems to be longer than the previous value. To verify this expectation, we carried out EPR measurements to directly determine $\tau_{\rm S}$.

The inset of Fig. 3(a) shows an EPR spectrum for a thick ($t_{\rm PE} = 10\ \mu$m) PEDOT:PSS film at room temperature. The spectrum fits the first derivative of a single Lorenz function (solid line). This fact means that the full width at the half maximum $\Delta H_{\rm EPR}$ is correlated with the spin-spin relaxation (or dephasing) time T_2 as in the relation $\Delta H_{\rm EPR} = 2/(\gamma T_2)$ with a gyromagnetic ratio of γ [31]. The present result ($\Delta H_{\rm EPR} = 24$ Oe) gives $T_2 = 4.7$ ns. However, the spin lifetime $\tau_{\rm S}$ responsible for the dc component of the spin current is the spin-lattice (or energy) relaxation time T_1, which is generally longer than T_2. We estimated T_1 by measuring the saturation behavior of the EPR intensity ($I_{\rm EPR}$) with a change in the microwave magnetic field ($h_{\rm ac}$) [31]. The main panel of Fig. 3(a) shows the $h_{\rm ac}$ dependence of $I_{\rm EPR}$. $I_{\rm EPR}$ has an almost linear dependence with $h_{\rm ac}$ and does not saturate even at maximum $h_{\rm ac}$. We also show the simulated results of the saturation curve with $h_{\rm ac}$ in Fig. 3(b). The comparison between these two figures suggests that T_1 is in the range of 5–100 ns and the lower limit of T_1 corresponds to the case where $T_1 = T_2$. This value is much shorter than the previously estimated $\tau_{\rm S}$ of 5–10 μs at room temperature [11]. In the previous study, $\tau_{\rm S}$ was

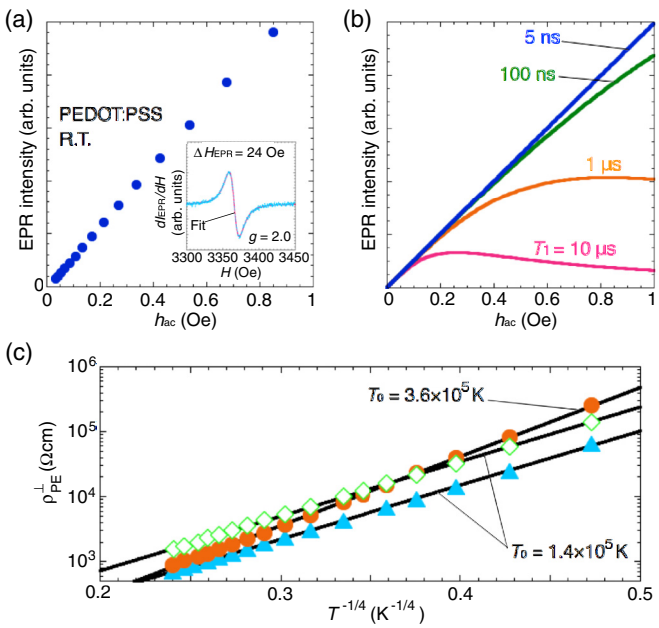

FIG. 3. (Color online) (a) Microwave magnetic field ($h_{\rm ac}$) dependence of the EPR intensity of a thick PEDOT:PSS film at room temperature. $h_{\rm ac}$ was calculated from the quality factor of the cavity. The intensity was obtained from the fitting as shown in the inset. Inset: The EPR spectrum for $h_{\rm ac} = 0.042$ Oe. The observed spectrum was fit to a single Lorenz function with a $\Delta H_{\rm EPR}$ of 24 Oe. (b) The simulated behavior of the EPR intensity as a function of $h_{\rm ac}$ for several values of T_1. The EPR intensity was calculated using $I_{\rm EPR} = h_{\rm ac}/\{1 + h^2_{\rm ac}\gamma^2 T_1 T_2\}$ with a fixed T_2 (=4.7 ns) [31]. (c) Temperature dependence of $\rho^{\perp}_{\rm PE}$ plotted with $T^{-1/4}$. We measured three distinct samples. The solid lines are fits based on the 3D-VRH.

indirectly estimated using the relation between the SDL and D_S, where $\tau_S = (\lambda^S)^2/D_S$ and assuming the Einstein relation for nondegenerate semiconductors with $D_S = \mu k_B T/e$, where μ is the mobility, k_B is the Boltzmann constant, and e is the elementary charge. The large discrepancy between τ_S of our experiment and the previous estimation suggests that the estimation of D_S using the Einstein relation for nondegenerate semiconductors is not applicable to the PEDOT:PSS film. Indeed, the Einstein relation to determine D_S has different forms depending on the conduction mechanism. For thermally excited transport (nondegenerate case), $D_S = \mu k_B T/e$ is applicable, but for highly doped semiconductors (degenerate case), D_S is inversely proportional to the resistivity (ρ) and the density of states at the Fermi level [$N(E_F)$], which is similar to metallic systems where $D_S = [e^2 N(E_F)\rho]^{-1}$.

We then measured the temperature dependence of the electrical resistivity to determine the conduction mechanism of PEDOT:PSS films. As shown in Fig. 3(c), the out-of-plane resistivity ($\rho_{PE}^{\perp}$) shows insulating behavior below room temperature and the logarithm of $\rho_{PE}^{\perp}$ is almost linear with $T^{-1/4}$, i.e., $\rho_{PE}^{\perp} \propto \exp(T_0/T)^{1/4}$. This is the characteristic behavior of three-dimensional variable range hopping (3D-VRH) conduction [32,33]. In VRH conduction, electron transport is not dominated by thermally excited charge carriers but by tunneling between metallic localized states. The characteristic temperature T_0 is expressed as $\beta/[k_B N(E_F)\xi^3]$ with constant $N(E_F)$, where β and ξ are the numerical factor ($\beta = 18.1$ for 3D case) and the localization length, respectively. This temperature-independent $N(E_F)$ is characteristic of degenerate systems and the Einstein relation for degenerate systems is applicable in the case of VRH conduction [34]. The localization length can be obtained from analysis of the current-voltage (I-V) characteristics in the perpendicular direction (see the Supplemental Material for details [30]), and then $N(E_F)$ can be calculated from T_0 and ξ. We measured three distinct samples and obtained the following average values: $\rho_{PE}^{\perp} = 1.0 \pm 0.4\ \mathrm{k\Omega\,cm}$, $N(E_F) = 8.8 \pm 7 \times 10^{17}\ \mathrm{eV^{-1}\,cm^{-3}}$, and $\xi = 11 \pm 4$ nm. These values are reasonably consistent with the previous study [13]. If we substitute the present values of ρ and $N(E_F)$ into the Einstein relation for degenerate systems, D_S was estimated to be $7.1 \pm 6 \times 10^{-7}\ \mathrm{m^2/s}$. This value leads to an estimated spin lifetime from the spin and charge transport experiments ($\tau_S^{\mathrm{transport}}$) of $\tau_S^{\mathrm{transport}} = (\lambda_{PE}^S)^2/D_S = 28 \pm 20$ ns.

We now relate $\tau_S^{\mathrm{transport}}$ to T_1 estimated from the EPR experiments. Because the present charge transport mechanism is dominated by VRH, $\tau_S^{\mathrm{transport}}$ contains contributions from spin relaxation during the hopping and trapping processes. In this case, the relation between $\tau_S^{\mathrm{transport}}$ and the spin relaxation rates is expressed as $1/\tau_S^{\mathrm{transport}} = 1/\tau_S^{\mathrm{hop}} + 1/\tau_S^{\mathrm{trap}}$. On the other hand, T_1 is almost equivalent to τ_S^{trap} because EPR experiments mainly probe electronic states inside the conducting polymer cores, i.e., $T_1 \approx \tau_S^{\mathrm{trap}}$ [35], and thus we obtain $1/\tau_S^{\mathrm{transport}} = 1/\tau_S^{\mathrm{hop}} + 1/T_1$. The present study shows that $\tau_S^{\mathrm{transport}}$ and T_1 are the same order of magnitude, implying that $\tau_S^{\mathrm{transport}} \approx T_1$ [36]. Therefore, we obtain $1/\tau_S^{\mathrm{hop}} \ll 1/\tau_S^{\mathrm{trap}}$: The spin relaxation mainly takes place during the trapping process. This expectation is consistent with the experimental result of $\lambda_{PE}^S > L_m$, where L_m is the average hopping length.

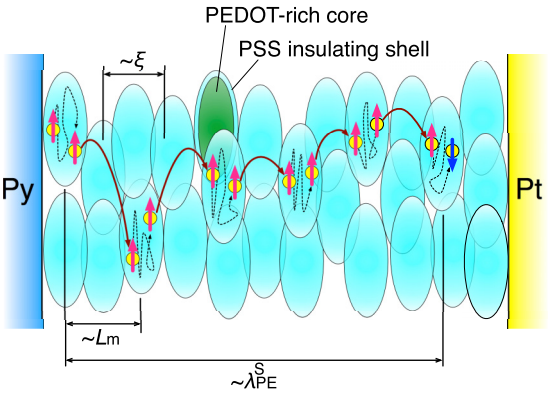

FIG. 4. (Color online) Schematic of the expected spin transport mechanism in the PEDOT:PSS film. The three characteristic lengths (ξ, L_m, and λ_{PE}^S) are also shown. Because λ_{PE}^S is longer than L_m, the spins are almost preserved through hopping. The spin relaxation during trapping process is enhanced by diffusive transport in the PEDOT-rich cores. Therefore, spin relaxation is likely to be dominated by spin relaxation in the cores.

From the I-V measurements, we estimated $L_m = 25 \pm 8$ nm at room temperature (see the Supplemental Material [30]). This value is five to six times smaller than λ_{PE}^S of 140 ± 20 nm. Therefore, the spin flip probability in the hopping event is much smaller than unity and spin angular momentum is almost conserved in the hopping process.

The previously reported spin transport experiment for another OSC suggests spin relaxation during the hopping process, where $1/\tau_S^{\mathrm{hop}} \gg 1/\tau_S^{\mathrm{trap}}$: Spin relaxation during the trapping process was not considered [12]. The OSC used in the previous report was not intentionally doped, therefore the electrons involved in the trapping process are localized and highly isolated from the spin relaxation path. This situation is completely different from the present case where the PEDOT molecule is highly doped with PSS. Because of the intensive doping, many conduction electrons exist in the PEDOT-rich cores, so that the spin relaxation rate during the trapping process is highly enhanced by diffusive transport in the cores [35]. A schematic of the expected spin transport mechanism in a PEDOT:PSS film is illustrated in Fig. 4.

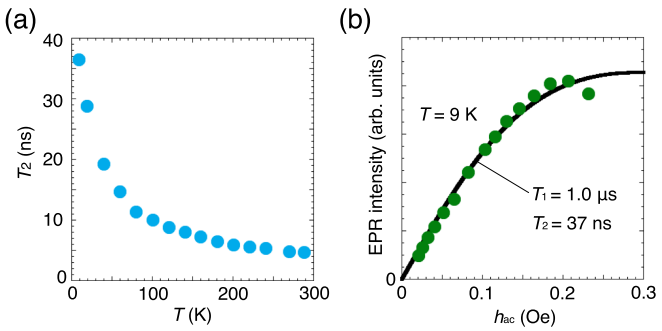

FIG. 5. (Color online) (a) Temperature dependence of T_2 evaluated from ΔH_{EPR}. (b) The h_{ac} dependence of the EPR intensity at 9 K. The solid line shows the saturation curve for $T_1 = 1.0$ μs and $T_2 = 37$ ns [31].

Next, we discuss the temperature dependence of spin relaxation. In OSCs, the dominant spin relaxation mechanism is still controversial, but two major candidates were proposed: the hyperfine (HF) interaction and SO coupling [37–39]. Figure 5(a) shows the temperature dependence of T_2 obtained from $\Delta H_{\mathrm{EPR}}(T)$. In this figure, T_2 gradually increased with a decrease in temperature, and reached 37 ns at 9 K. Also, the saturation behavior of I_{EPR} at 9 K gives a T_1 of 1 μs [Fig. 5(b)]. These results indicate that $\tau_{\mathrm{S}}^{\mathrm{EPR}}$ of PEDOT:PSS increases at low temperatures. As discussed in Ref. [35], this result clearly indicates that spin relaxation is caused by the spin-lattice relaxation via SO coupling between the polymer back bone and the conduction electrons. The effect of the HF interaction would not be dominant in the present case because HF coupling in organic materials is weak, and the magnitude of the HF field amounts to a few tens of oersted [40]. Therefore, the spin relaxation (or dephasing) originating from the HF field is suppressed at sufficiently high magnetic fields ($\gtrsim$1000 Oe in the present experiments). The spin relaxation because of the HF interaction, on the other hand, should be considered at very low magnetic fields and in a material with weak SO coupling [41].

Finally, we mention the future prospects to enhance the SDLs of OSCs. The present study suggests that SO coupling is the dominant origin of the spin relaxation process even in organic materials. In PEDOT:PSS, the largest SO contribution is likely to arise from coupling with sulfur atoms, which is the heaviest atom in the thiophene framework. Hence, using light elements as a molecular building block is a straightforward way to achieve a longer τ_{S}. Another way would be to reduce the dopant concentration within the degenerate regime. As theoretically predicted, D_{S} is considerably enhanced by carrier doping, which induces crossover from the nondegenerate regime to the degenerate regime [42]. Therefore, the existence of degenerate charge carriers is quite important to realize a large D_{S}. Based on the Einstein relation for degenerate systems, large D_{S} can be obtained by reducing $N(E_{\mathrm{F}})$, i.e., reducing the doping concentration. Also, τ_{S} depends on the doping concentration. The *in situ* EPR experiment as a function of doping concentration showed that the EPR linewidth decreased as the doping concentration was lowered [43]. This indicates that τ_{S} is increased by reducing the doping. These discussions are qualitatively consistent with the different SDLs of the present and the previous studies: The present SDL of $\sim$140 nm on average is rather long compared with the previously reported value of 21–30 nm [11]. This discrepancy is probably because of the difference in doping concentration in PEDOT:PSS. The material used in the previous report was also doped with dimethyl sulfoxide solvents.

IV. CONCLUSIONS

We performed dynamical pure spin current transport, EPR, and charge transport experiments in a film of the highly doped organic polymer PEDOT:PSS. The obtained $\tau_{\mathrm{S}}^{\mathrm{transport}}$ from spin and charge transport experiments was much shorter than the previous report for nondoped OSCs. Therefore, this $\tau_{\mathrm{S}}^{\mathrm{transport}}$ was caused by intentional hole doping in the PEDOT molecule. Because the PEDOT molecules are concentrated at the PEDOT-rich core, $\tau_{\mathrm{S}}^{\mathrm{transport}}$ is dominated by the τ_{S} at the core, i.e., the trapping center. Indeed, T_1 obtained from the EPR experiment, which mainly probes τ_{S} inside the cores, was comparable to $\tau_{\mathrm{S}}^{\mathrm{transport}}$. Also, we found that the SDL was longer than the average hopping length, meaning that the spin angular momentum is almost preserved during the hopping process. Based on these discussions, spin relaxation in the PEDOT:PSS film mostly takes place while the carrier is trapped in the core. The temperature dependence of the EPR experiment shows that the main spin relaxation mechanism of this material is spin-lattice relaxation caused by SO coupling. These conclusions will contribute to the full understanding of pure spin current transport in organic semiconductors.

ACKNOWLEDGMENTS

The authors acknowledge T. Kato, H. Tanaka, T. Sasaki, Y. Honma, S. Watanabe, and K. Furukawa for helpful discussions. The authors also acknowledge R. Takahashi and M. Lippmaa for the use of a surface profile measurement system. This work was partly supported by a Grant-in-Aid for Challenging Exploratory Research (No. 24654100) and Scientific Research on Innovative Area, "Nano Spin Conversion Science" (No. 26103002) from Japan Society of the Promotion of the Science (JSPS).

[1] I. Žutić, J. Fabian, and S. D. Sarma, Rev. Mod. Phys. **76**, 323 (2004).
[2] V. A. Dediu, L. E. Hueso, I. Bergenti, and C. Taliani, Nat. Mater. **8**, 707 (2009).
[3] V. A. Dediu, M. Murgia, F. C. Matacotta, C. Taliani, and S. Barbanera, Solid State Commun. **122**, 181 (2002).
[4] Z. H. Xiong, D. Wu, Z. V. Vardeny, and J. Shi, Nature (London) **427**, 821 (2004).
[5] N. A. Morley, A. Rao, D. Dhandapani, M. R. J. Gibbs, M. Grell, and T. Richardson, J. Appl. Phys. **103**, 07F306 (2008).
[6] T. S. Santos, J. S. Lee, P. Migdal, I. C. Lekshmi, B. Satpati, and J. S. Moodera, Phys. Rev. Lett. **98**, 016601 (2007).
[7] T. D. Nguyen, F. Wang, X.-G. Li, E. Ehrenfreund, and Z. V. Vardeny, Phys. Rev. B **87**, 075205 (2013).
[8] J. H. Shim, K. V. Raman, Y. J. Park, T. S. Santos, G. X. Miao, B. Satpati, and J. S. Moodera, Phys. Rev. Lett. **100**, 226603 (2008).
[9] Y. Fukuma, L. Wang, H. Idzuchi, S. Takahashi, S. Maekawa, and Y. Otani, Nat. Mater. **10**, 527 (2011).
[10] H. Idzuchi, Y. Fukuma, and Y. Otani, Sci. Rep. **2**, 628 (2012).
[11] K. Ando, S. Watanabe, S. Mooser, E. Saitoh, and H. Sirringhaus, Nat. Mater. **12**, 622 (2013).
[12] S. Watanabe, K. Ando, K. Kang, S. Mooser, Y. Vaynzof, H. Kurebayashi, E. Saitoh, and H. Sirringhaus, Nat. Phys. **10**, 308 (2014).
[13] A. M. Nardes, R. A. J. Janssen, and M. Kemerink, Adv. Funct. Mater. **18**, 865 (2008).
[14] T. Takano, H. Masunaga, A. Fujiwara, H. Okuzaki, and T. Sasaki, Macromolecules **45**, 3859 (2012).

[15] R. H. Silsbee, A. Janossy, and P. Monod, Phys. Rev. B **19**, 4382 (1979).
[16] S. Mizukami, Y. Ando, and T. Miyazaki, Phys. Rev. B **66**, 104413 (2002).
[17] Y. Tserkovnyak, A. Brataas, and G. E. W. Bauer, J. Appl. Phys. **93**, 7534 (2003).
[18] E. Saitoh, M. Ueda, H. Miyajima, and G. Tatara, Appl. Phys. Lett. **88**, 182509 (2006).
[19] S. O. Valenzuela and M. Tinkham, Nature (London) **442**, 176 (2006).
[20] T. Kimura, Y. Otani, T. Sato, S. Takahashi, and S. Maekawa, Phys. Rev. Lett. **98**, 156601 (2007).
[21] N. Mecking, Y. S. Gui, and C.-M. Hu, Phys. Rev. B **76**, 224430 (2007).
[22] M. Harder, Z. X. Cao, Y. S. Gui, X. L. Fan, and C.-M. Hu, Phys. Rev. B **84**, 054423 (2011).
[23] A. Azevedo, L. H. Vilela-Leão, R. L. Rodríguez-Suárez, A. F. Lacerda Santos, and S. M. Rezende, Phys. Rev. B **83**, 144402 (2011).
[24] L. Bai, Z. Feng, P. Hyde, H. F. Ding, and C.-M. Hu, Appl. Phys. Lett. **102**, 242402 (2013).
[25] H. Chen, X. Fan, H. Zhou, W. Wang, Y. S. Gui, C.-M. Hu, and D. Xue, J. Appl. Phys. **113**, 17C732 (2013).
[26] K. Ando, S. Takahashi, J. Ieda, Y. Kajiwara, H. Nakayama, T. Yoshino, K. Harii, Y. Fujikawa, M. Matsuo, S. Maekawa, and E. Saitoh, J. Appl. Phys. **109**, 103913 (2011).
[27] L. Chen, S. Ikeda, F. Matsukura, and H. Ohno, Appl. Phys. Express **7**, 013002 (2014).
[28] R. Iguchi, K. Sato, D. Hirobe, S. Daimon, and E. Saitoh, Appl. Phys. Express **7**, 013003 (2014).
[29] O. Mosendz, V. Vlaminck, J. E. Pearson, F. Y. Fradin, G. E. W. Bauer, S. D. Bader, and A. Hoffmann, Phys. Rev. B **82**, 214403 (2010).
[30] See Supplemental Material at http://link.aps.org/supplemental/10.1103/PhysRevB.91.224422 for additional supporting information and details of analysis methods.
[31] C. P. Poole and H. A. Farach, *Relaxation in Magnetic Resonance* (Academic, New York, 1971).
[32] N. F. Mott, J. Non-Cryst. Solids **1**, 1 (1968).
[33] B. I. Shklovskii and A. L. Efros, *Electronic Properties of Doped Semiconductors* (Springer, Berlin, 1983).
[34] G. Paascha, T. Lindnera, and S. Scheinert, Synth. Met. **132**, 97 (2002).
[35] K. Mizoguchi, M. Honda, N. Kachi, F. Shim, H. Sakamoto, K. Kume, S. Masubuchi, and S. Kazama, Solid State Commun. **96**, 333 (1995).
[36] Due to the experimental ambiguity, it is possible to consider the cases of $1/\tau_S^{hop} < 1/\tau_S^{trap}$ and $1/\tau_S^{hop} > 1/\tau_S^{trap}$ for the arbitrary magnitude relation between $\tau_S^{transport}$ and T_1. However, $\tau_S^{transport}$ of $\sim$28 ns is much shorter than that found in nondoped OSCs [3, 8]. Therefore, this short $\tau_S^{transport}$ is likely arising from intensive hole doping into the PEDOT molecules. In the PEDOT:PSS film, the PEDOT molecules concentrate at the PEDOT-rich cores, so $\tau_S^{transport}$ is likely dominated by τ_S in the cores, i.e., $\tau_S^{transport} \approx \tau_S^{trap}$.
[37] P. A. Bobbert, W. Wagemans, F. W. A. van Oost, B. Koopmans, and M. Wohlgenannt, Phys. Rev. Lett. **102**, 156604 (2009).
[38] Z. G. Yu, Phys. Rev. Lett. **106**, 106602 (2011).
[39] N. J. Harmon and M. E. Flatté, Phys. Rev. Lett. **110**, 176602 (2013).
[40] W. J. M. Naber, S. Faez, and W. G. van der Wiel, J. Phys. D: Appl. Phys. **40**, R205 (2007).
[41] T. D. Nguyen, G. H. Markosian, F. Wang, L. Wojcik, X.-G. Li, E. Ehrenfreund, and Z. V. Vardeny, Nat. Mater. **9**, 345 (2010).
[42] M. E. Flatté and J. M. Byers, Phys. Rev. Lett. **84**, 4220 (2000); Y. Q. Peng, J. H. Yang, F. P. Lu, Q. S. Yang, H. W. Xing, X. S. Li, and C. A. Song, Appl. Phys. A **86**, 225 (2006); Y. Roichman and N. Tessler, Appl. Phys. Lett. **80**, 1948 (2002).
[43] A. Zykwinska, W. Domagala, and M. Lapkowski, Electrochem. Commun. **5**, 603 (2003).